SLAC-PUB-17271

Bunching phase and constraints on echo enabled harmonic generation

E. Hemsing
SLAC National Accelerator Laboratory,
Menlo Park, California 94025, USA
(Dated: May 28, 2018)

Abstract

A simple mathematical description is developed for the bunching spectrum in echo enabled harmonic generation (EEHG) that incorporates the effect of additional electron beam energy modulations. Under common assumptions, they are shown to contribute purely through the phase of the longitudinal bunching factor, which allows the spectral moments of the bunching to be calculated directly from the known energy modulations. In particular, the second moment (spectral bandwidth) serves as simple constraint on the amplitude of the energy modulations to maintain a transform-limited seed. We show that, in general, the impact on the spectrum of energy distortions that develop between the EEHG chicanes scales like the harmonic number compared to distortions that occur upstream. This may limit the parameters that will allow EEHG to reach short wavelengths in high brightness FELs.

This material is based upon work supported by the U.S. Department of Energy,
Office of Science, under Contract No. DE-AC02-76SF00515.

I. INTRODUCTION

Echo Enabled Harmonic Generation (EEHG)[1] is an external seeding scheme for modern free electron lasers (FELs) designed to improve the temporal coherence and produce a transform-limited output pulse. It uses lasers to imprint coherent energy modulations on a relativistic electron beam that are then converted to a high harmonic density modulation. The beam then enters the FEL undulator where the density-modulated (bunched) electrons radiate coherently, and the radiation is amplified up to saturation. To reach EUV or shorter wavelengths from conventional UV lasers, high harmonics with EEHG are required, but preservation of the coherent modulation can be challenging during the manipulation and transport.

As with most harmonic up-conversion schemes, initial errors can be multiplied and spoil the final output. The sensitivity of EEHG to initial laser phase, noise, and energy distortions in the electron beam has been examined previously [2–8]. EEHG uses two laser modulators and two dispersive chicanes to perform the harmonic upshift, and the final bunching spectrum is relatively insensitive to small distortions on the beam or in the laser upstream of the first chicane [9, 10]. Laser phase distortions in the second modulator, however, can get amplified and impact the time-bandwidth product similarly to High Gain Harmonic Generation (HGHG) [11].

Here we examine the impact of energy structures on the beam that emerge during the EEHG transformation i.e., between the chicanes. Such energy distortions can be particularly problematic because much like phase errors in the second laser, they are not filtered by the large first dispersion and have a pronounced impact on the final spectrum. To analyze the problem, we develop a general description for the bunching in the presence of small but arbitrary energy modulations. Simple distortions are analyzed and compared with previous results. We then consider the impact on the bunching spectrum of two common contributors to nonlinear beam energy structure; longitudinal space charge (LSC) and coherent synchrotron radiation (CSR). Both are driven by collective effects and are difficult to remove. LSC produces energy modulations from localized density perturbations and from the beam core itself. For highly relativistic beams in a short drift the modulations are negligible, but in strong modulators $K_u \gg 1$, the effective drift length can increase by $\sim K_u^2$ which may be on the order of a kilometer for few GeV-scale beams coupling to UV lasers. This can have a significant impact on the final bunching in EEHG. Alternately, CSR leads to nonlinear energy structures from the coherent emission of the beam as it bends through magnetic dipoles. This has the largest impact on the bunching in the last two bends of the strong first EEHG chicane. Here, for both LSC and CSR, constraints on the induced energy structures according to their impact on the bunching spectrum are derived with simple models, and results are checked with numerical particle simulations. General limits are established on the relevant parameters to seed transform-limited FEL pulses with EEHG.

II. MATHEMATICAL DESCRIPTION

Notation closely follows that of [12] where more details on the EEHG process can be found. Consider an electron beam transformation similar to EEHG of the form,

$$\begin{aligned} p_1 &= p + A_1 \sin(k_1 z) + \Delta p_1(z), \\ z_1 &= z + B_1 p_1/k_1, \\ p_2 &= p_1 + A_2 \sin(k_2 z_1) + \Delta p_2(z_1), \\ z_2 &= z_1 + B_2 p_2/k_1. \end{aligned} \tag{1}$$

where the normalized laser modulations are $A_{1,2} = \Delta\gamma_{1,2}/\sigma_\gamma$, normalized dispersions are $B_{1,2} = k_1 R_{56}^{(1,2)} \sigma_\gamma/\gamma$, the slice energy spread is σ_γ, and γ is the relativistic factor. Additional energy modulations Δp_1 and Δp_2 of arbitrary longitudinal dependence are modeled as occurring alongside the laser modulations. In this simplified description, Δp_1 can also be any existing energy structure from upstream, and Δp_2 can be used to capture the integrated effect of CSR from the first chicane.

In a beam with the phase space distribution $f(z,p)$, the bunching spectrum near the harmonic spatial frequency $k_E = a_E k_1 = (n + mK)k_1$ is given by

$$\begin{aligned} b_{n,m}(k) = \int & e^{-iz(k-k_E) - i\xi p - i\xi \Delta p_1(z) - ikB_2 \Delta p_2(z_1)/k_1} \\ & \times f(z,p) J_n(-\xi A_1) J_m(-kA_2 B_2/k_1) dz dp, \end{aligned} \tag{2}$$

where $\xi = kB/k_1 - mKB_1$, $B = B_1 + B_2$, and $K = k_2/k_1$. Useful analytic solutions for $b_{n,m}(k)$ are available only for a few simple forms of the energy modulations, particularly for Δp_2 which is a function of $z_1(z,p)$ rather than z. However, if Δp_2 is sufficiently slowly-varying that the modulation experienced at the position z_1 is the same as at z, then $\Delta p_2(z_1) = \Delta p_2(z)$ is a significant mathematical simplification. Similarly, we also assume that the energy structures in Δp_1 are small enough so that they do not lead to large changes in the phase space distribution after the first chicane, $B_1 d\Delta p_1/dz \ll k_1$. We will explore these assumptions shortly. Retaining the lowest order contributions near the harmonic, the bunching spectrum can be written as

$$b_{n,m}(k) \approx \bar{b}_{n,m} \int f(z) e^{-iz(k-k_E) + i\varphi(z)} dz, \tag{3}$$

where $\bar{b}_{n,m} = e^{-\xi_E^2/2} J_n(-\xi_E A_1) J_m(-a_E A_2 B_2)$ is the optimized bunching amplitude and $\xi_E = nB_1 + a_E B_2$ is the EEHG scaling parameter [10]. An uncorrelated Gaussian initial energy distribution $f(z,p) = f(z)(2\pi)^{-1/2} e^{-p^2/2}$ has been assumed. The additional energy modulations Δp_1 and Δp_2 are expressed through a z-dependent phase,

$$\begin{aligned} \varphi(z) &= -\xi_E \Delta p_1(z) - a_E B_2 \Delta p_2(z) \\ &= \varphi_1(z) + \varphi_2(z). \end{aligned} \tag{4}$$

Evidently, energy modulations that occur within or before the first modulator, Δp_1, are multiplied by the small scaling parameter $|\xi_E| \lesssim 1$ in their contribution to the phase $\varphi_1(z)$. Linear, quadratic, and sinusoidal such initial modulations were studied in [10], where it was shown that the smallness of ξ_E is responsible for the relative insensitivity of the EEHG

bunching spectrum to small initial perturbations. However, we see here that energy modulations introduced between the chicanes, Δp_2, are multiplied by the much larger factor $a_E B_2 \approx m/A_2 \gg 1$ and therefore can have a pronounced impact on the final bunching spectrum at high harmonics.

From (3), the bunching along z can be identified from the Fourier transform $b_{n,m}(k) = \int \tilde{b}_{n,m}(z) e^{-ikz} dz$:

$$\tilde{b}_{n,m}(z) = \bar{b}_{n,m} f(z) e^{ik_E z + i\varphi(z)}. \tag{5}$$

In this form it is straightforward to obtain both the instantaneous (local) and projected (global) behavior of the bunching spectrum. The instantaneous spatial bunching frequency is just the z-derivative of the full longitudinal phase,

$$k_z(z) = k_E + \varphi'(z). \tag{6}$$

Thus the local bunching frequency in the beam is calculated directly from the derivative of the energy modulations in (4) without the need to first solve for the bunching spectrum. From the instantaneous frequency we can then obtain the global mean frequency [13],

$$\langle k_z \rangle = \frac{\int_{-\infty}^{\infty} k_z(z) f^2(z) dz}{\int_{-\infty}^{\infty} f^2(z) dz} = k_E + \langle \varphi'(z) \rangle. \tag{7}$$

This is the first moment of the bunching spectrum, but here it is calculated simply from the beam distribution $f(z)$ and the additional phase. The bandwidth of $|b_{n,m}(k)|^2$ about $\langle k_z \rangle$ is then given by $\langle [k_z - \langle k_z \rangle]^2 \rangle$ [14]:

$$\begin{aligned} \sigma_k^2 &= \sigma_{k_E}^2 + \langle [\varphi' - \langle \varphi' \rangle]^2 \rangle, \\ &= \sigma_{k_E}^2 + \sigma_{\varphi'}^2, \end{aligned} \tag{8}$$

where $\sigma_{k_E}^2 = \int (f')^2 dz / \int f^2 dz$ yields the transform-limited bandwidth in the absence of additional energy structure. We define $\sigma_{\varphi'}$ as the bandwidth associated with the additional frequencies introduced through the phase $\varphi(z)$. It is particularly useful for capturing the influence of nonlinear low frequency modulations $\mathcal{O}(1/\sigma_z)$ that broaden the bandwidth and produce a pedestal near the bunching harmonic. To maintain high quality FEL seeding in the presence of such bandwidth growth, one figure of merit on the magnitude of the tolerable energy modulations on the beam is then

$$\sigma_{\varphi'} / \sigma_{k_E} \leq 1. \tag{9}$$

This will be used throughout, and states that the additional bandwidth should be less than the bandwidth of the bunching spectrum defined by the unperturbed beam.

Visualization of the instantaneous bunching spectrum is assisted by a Wigner distribution,

$$W(z,k) = \int_{-\infty}^{\infty} e^{-ikx} \tilde{b}_{n,m}(z + x/2) \tilde{b}_{n,m}^*(z - x/2) dx. \tag{10}$$

The bunching spectral power is $|b_{n,m}(k)|^2 = \int_{-\infty}^{\infty} W(z,k) dz$, and the instantaneous frequency is the average frequency of $W(z,k)$ at a given z position, $k_z(z) = \int_{-\infty}^{\infty} k W(z,k) dk / \int_{-\infty}^{\infty} W(z,k) dk$ [15].

One measure of how accurately the approximate bunching in (3) reproduces the exact solution in (2) is the harmonic shift of the bunching peak in a beam with a linear energy chirp, which can be solved exactly in both cases. An initial linear chirp of the form $\Delta p_1 = h_1 k_1 z$ was solved explicitly in [9, 10] and yields a shifted harmonic factor of $a = (a_E + mKh_1B_1)/(1 + h_1B)$. From Eq. (7) with $\langle\varphi'(z)\rangle = -\xi_E h_1 k_1$, the shifted harmonic in the approximate theory is $a = a_E - \xi_E h_1$. The relative difference between the two appears only to second order in the chirp, $h_1^2\xi_E B/a_E$, which is generally small. An identical chirp acquired in the second modulator $\Delta p_2 = h_1 k_1 z$ yields $a = a_E/(1+h_1B_2)$ from the exact expression in (2), or $a = a_E(1 - h_1B_2)$ from the approximate expression in (7). Similarly, the relative difference to lowest order is $h_1^2B_2^2$, which is also typically small.

With this approximate description we can compute the spatial-spectral distribution of the bunching through the shape of the energy modulations imprinted on the beam. Two simple examples with analytic solutions are given in the Appendix. More complicated nonlinear modulations generated by LSC and CSR are examined in the following sections.

III. LONGITUDINAL SPACE CHARGE

LSC generates energy structures from the mutual repulsion of electrons near density peaks. In a cylindrical beam with uniform transverse density and hard-edge radius r_b, the on-axis energy change over the length L_d due to LSC forces is

$$\Delta p_{LSC}(z) = \frac{4L_d}{\sigma_\gamma}\int_0^\infty \frac{Z(k)}{iZ_0}dk \int_{-\infty}^{\infty}\frac{I(z')}{I_A}\sin[k(z-z')]dz' \tag{11}$$

where I_A=17 kA, $Z_0 = 377\ \Omega$, and $I(z) = Qcf(z)$ is the current profile. The LSC impedance per unit length $Z(k)$ depends on the parameters of the system [16]. Inside an undulator and under specific conditions, the impedance can be strongly enhanced compared to a free space drift [17]. Assuming these conditions are satisfied for the EEHG modulators and in the limit $kr_b/\gamma_z \ll 1$,

$$Z(k) = \frac{iZ_0 k}{4\pi\gamma_z^2}\left[1 + 2\ln\left(\frac{\gamma_z}{kr_b}\right)\right], \tag{12}$$

where $\gamma_z = \gamma/\sqrt{1 + K_u^2/2}$ is the longitudinal Lorentz factor inside an undulator.

Assuming a Gaussian current profile $I(z) = I_0 e^{-z^2/2\sigma_z^2}$ for a pencil beam $r_b/\gamma\sigma_z \ll 1$, the associated energy modulation is,

$$\Delta p_{LSC}(z) \approx \frac{2I_0 L_d z}{\sigma_\gamma I_A \gamma_z^2 \sigma_z^2}\ln\left(\frac{\gamma_z\sigma_z}{r_b}\right)e^{-z^2/2\sigma_z^2}. \tag{13}$$

The shape of the modulation is shown in FIG. 1. The long-range LSC wake generates a positive energy chirp in the beam core. If it develops in the second modulator, it redshifts the local bunching frequency as indicated by $k_z(z)$, which is calculated from $\Delta p_{LSC}(z)$ with Eqs. (4) and (6). The LSC-induced bandwidth constraint from (9) with $\sigma_{k_E} = 1/\sqrt{2}\sigma_z$ for a Gaussian is

$$\sigma_{\varphi'_{LSC}}/\sigma_{k_E} \approx \eta\frac{I_0 L_d}{\sigma_\gamma I_A \gamma_z^2 \sigma_z}\ln\left(\frac{\gamma_z\sigma_z}{r_b}\right) \le 1 \tag{14}$$

where $\eta = \xi_E$ or $a_E B_2$ depending on whether the LSC effect occurs in the first or second modulator, respectively. Inspection of the induced global energy spread $\sigma_{\Delta p_{LSC}} \approx \sigma_{\varphi'_{LSC}}\sigma_z/\eta$

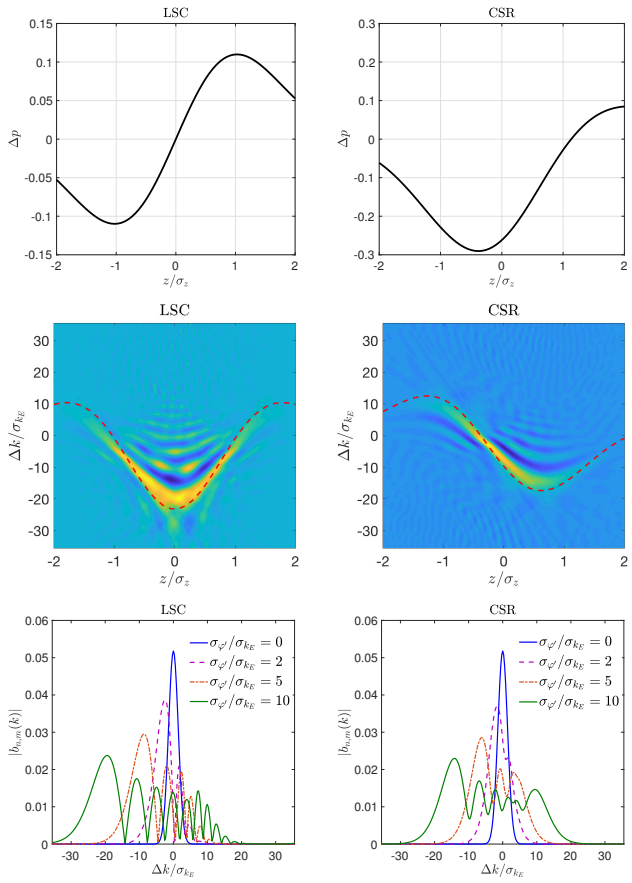

FIG. 1: Examples of LSC and CSR wakes (top), Wigner bunching distributions (middle), and bunching spectra (bottom). The instantaneous frequency from theory is plotted (dashed red line) over each Wigner distribution, which are from numerical simulations of the case when $\sigma_{\varphi'}/\sigma_{k_E} = 10$. Results apply generally for Gaussian beams with energy structures described by Eqs. (13) and (22).

shows that Eq. (14) translates to a simple constraint; $\sigma_{\Delta p_{LSC}} \leq 1/\sqrt{2}\eta$. Clearly if $\eta = a_E B_2 \gg 1$, the tolerable energy modulation from LSC in the second modulator is much less than the intrinsic slice energy spread. This may be problematic for high current beams in strong undulators.

IV. MICROBUNCHING INSTABILITY

Consider a beam upstream of the EEHG line with a small amplitude ($b_0 \ll 1$) density modulation $I(z) = I_0(1 + 2b_0 \cos k_0 z)$ that gets amplified by LSC and produces an energy modulation. Through a drift length (or undulator) L_d, space charge forces will drive energy modulations with frequency $k_0 \gg 1/\sigma_z$ according to [18],

$$\begin{aligned} \Delta p_M(z) &= \frac{8\pi b_0 I_0 L_d |Z(k_0)|}{\sigma_\gamma I_A Z_0} \sin(k_0 z) \\ &= A_M(k_0) \sin(k_0 z). \end{aligned} \tag{15}$$

In the limit $k_0 \ll k_1$ a monochromatic modulation generates coherent bunching sidebands at the frequencies $k_E \pm q k_0$ with amplitudes that scale as $J_q(\eta A_M)$. The case of an energy

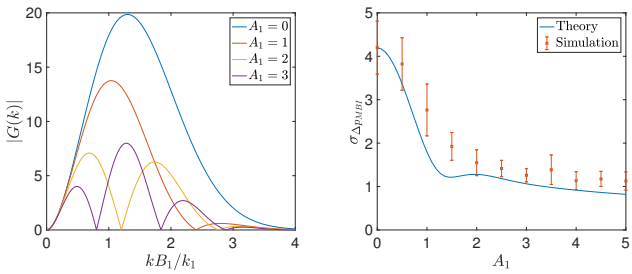

FIG. 2: Left: Density modulation gain function through the first EEHG modulator and chicane. Right: Corresponding impact of A_1 on the MBI-induced energy spread through the second undulator with $A_M(k_m) = 0.17$, $A_{M,2}(k_m) = 0.11$, and $b_0 = 0.2\%$. Parameters are similar to an idealized LCLS-II, 4 GeV beam at high current $I_0 = 3.3$ kA to exaggerate the effect for simulation efficiency, with $\sigma_\gamma = 0.88$, $\sigma_z/c = 50$ fs, $r_b = 30$ μm, $L_{d,1} = 6.25$ m, $L_{d,2} = 4$ m, $K_u = 17.8$, $B_1 = 20$, and $2\pi/k_1 = 260$ nm.

modulation upstream of the first chicane ($\eta = \xi_E$) was studied in [10]. Here we see that if the energy modulation develops in the second modulator, the larger $\eta = a_E B_2 \gg 1$ leads to a much stronger effect on the spectrum. For example, the bunching at k_E is suppressed when $J_0(\eta A_M) = 0$, and thus when $A_M = 2.4/\eta$. Clearly if $\eta = a_E B_2$ this can be much smaller than the slice energy spread.

Let us assume that the energy modulation in (15) occurs in the first EEHG modulator alongside the first laser modulation. The beam will then pass through the first EEHG chicane, which can convert the induced energy modulation into a density modulation, depending on k_0. Higher frequencies can be suppressed [19], whereas lower frequencies can be amplified. In the linear theory, the current spectrum after the chicane is just the initial current spectrum times a density "gain" function,

$$G(k_0) = -\frac{k_0 B_1}{2k_1 b_0} A_M(k_0) J_0\left(\frac{k_0 B_1}{k_1} A_1\right) e^{-\frac{1}{2}\left(\frac{k_0 B_1}{k_1}\right)^2} \tag{16}$$

where $b_0 \ll \frac{k_0 B_1}{k_1} A_M < 1$. In the absence of the first laser $A_1 = 0$, this reduces to the standard expression for the gain due to LSC [20]. We see here however, that the first EEHG laser acts to reduce the growth of the density modulation (FIG. 2). It does so by mixing high frequency energy structures into the beam that are longitudinally smeared, similar to a laser heater.

In the second EEHG modulator, the density modulation can then develop into an additional energy modulation that will impact the spectrum via the phase $\varphi_2(z)$. The modulation at the end of the second undulator is similar to Eq. (15) but with the bunching multiplied by the gain,

$$\Delta p_{M,2}(z) = A_{M,2}(k_0) G(k_0) \sin(k_0 z). \tag{17}$$

$A_{M,2}$ has the same form as A_M but uses the impedance $L_d|Z(k_0)|$ of the second undulator. For $A_1 = 0$ the modulation scales in frequency as $\Delta p_{M,2} \propto k_0^3 e^{-(k_0 B_1/k_1)^2/2}$, which has maximum when $k_0 \approx k_m = \sqrt{3} k_1/B_1$. The EEHG beamline works as a LSC amplifier with multiple stages, but with the first laser and strong chicane providing some mitigation against MBI growth.

The single frequency analysis can be extended to the case of a beam that initially has a broadband spectrum of incoherent density modulations. Such is the case of MBI from

shot noise that can produce a spectral pedestal around the harmonic bunching spike [21]. This case can be modeled with (17) as a discrete sum over the different frequencies and corresponding amplitudes,

$$\Delta p_{MBI}(z) = \sum_j A_{M,2}(k_j) G(k_j) \sin(k_j z + \phi_j) \tag{18}$$

where ϕ_j is a random phase. For noise, the induced energy spread is dominated by the incoherent contribution to the sum, $\sigma^2_{\Delta p_{MBI}} = \frac{1}{2}\sum_j A_{M,2}(k_j)^2 G(k_j)^2$. The contribution to the bunching spectrum pedestal from the growth in the second modulator alone is then $\sigma^2_{\varphi'_{MBI}} = \frac{(a_E B_2)^2}{2}\sum_j A_{M,2}(k_j)^2 G(k_j)^2 k_j^2$. In the continuous limit we can integrate over the frequencies $\sigma^2_{\Delta p_{MBI}} = \frac{1}{2n_z}\int_0^\infty A_{M,2}(k)^2 G(k)^2 dk$ to obtain $\sigma^2_{\Delta p_{MBI}} \approx \frac{15k_1\sqrt{\pi}}{32 n_z B_1}\left(\frac{A_M A_{M,2}}{6b_0}\right)^2 {}_2F_2\left(\frac{1}{2},\frac{7}{2};1,1;-A_1^2\right)$ where A_M and $A_{M,2}$ are evaluated at the frequency peak k_m, and $n_z = \sqrt{2\pi}/\sigma_z$ for a Gaussian current. ${}_2F_2$ is a generalized hypergeometric function that captures the impact of A_1 on the MBI-driven energy spread growth, as shown in FIG. 2. If $A_1 > 2$ the energy spread growth is simply,

$$\sigma^2_{\Delta p_{MBI}} \approx \frac{k_1}{2\pi n_z B_1 A_1}\left(\frac{A_M A_{M,2}}{6b_0}\right)^2. \tag{19}$$

This expression holds if the energy modulations that develop from pure noise in the second modulator are small compared with those amplified through cascading, and the system satisfies the linear gain theory. Performing a similar integral for $\sigma_{\varphi'_{MBI}}$, one can obtain a relationship between the induced incoherent bandwidth growth and the induced incoherent energy spread growth. With $A_1 > 2$ it reduces to a simple form,

$$\sigma_{\varphi'_{MBI}}/\sigma_{k_E} \approx \sqrt{6}|n|k_1\sigma_z\sigma_{\Delta p_{MBI}}, \tag{20}$$

where $a_E B_2/B_1 \approx |n|$.

The constraint in Eq. (9) then gives $\sigma_{\Delta p_{MBI}} \leq 1/\sqrt{6}|n|k_1\sigma_z$, which is independent of the harmonic number and suggests that the MBI-induced energy spread through the second modulator must be much less than the slice energy spread (since $k_1\sigma_z \gg 1$) to maintain narrowband bunching. One caveat, however, is that $\sigma_{\varphi'_{MBI}}$ includes frequencies that may be outside the FEL bandwidth that can be largely ignored, specifically if $1/a_E B_1 > \rho$ or if the wavelengths are shorter than the cooperation length. Only when the MBI gain in the low frequencies near the spike is large enough does the bunching spectrum have an attached pedestal and the constraint applies.

FIG. 3 illustrates the impact of MBI on the bunching spectrum. Numerical simulations were performed with energy modulations imposed on the beam according to (18). Results of the bunching spectrum bandwidth indicate good agreement with the scaling of the incoherent energy spread in Eq. (20). Simulations also confirm that the bunching factor is reduced by $e^{-\frac{1}{2}(a_E B_2)^2\sigma^2_{\Delta p_{MBI}}}$ [22], and thus that the harmonic number is limited by the induced incoherent energy spread. Results highlight the need to keep b_0 as small as possible to avoid MBI growth in the EEHG section.

V. COHERENT SYNCHROTRON RADIATION

The impact of CSR on the EEHG bunching spectrum has been studied numerically (see, e.g., [23]). The energy modulation imparted by CSR along the beam after passage through

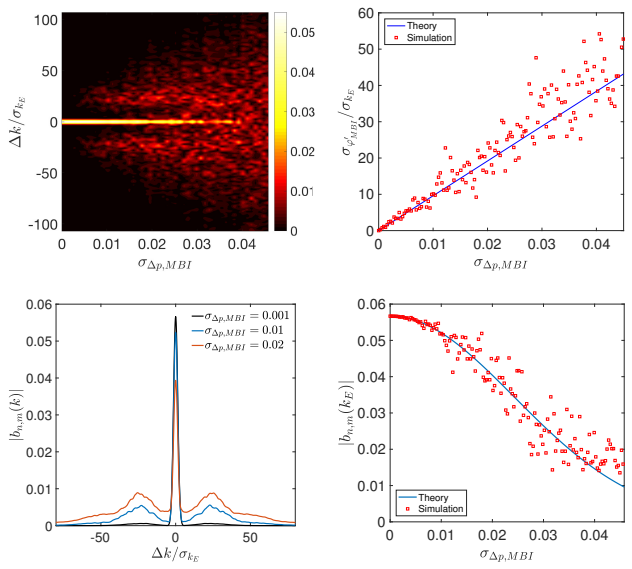

FIG. 3: MBI impact on EEHG bunching for parameters of an idealized LCLS-II type 4 GeV beam with $I_0 = 1$ kA, $A_1 = 3$, $A_2 = 5$, and $a_E = 200$, $n = -1$ using $2\pi/k_1 = 260$ nm seed lasers. Top left: Bunching spectrum evolution as a function of MBI-induced energy spread. Top right: Corresponding induced spectral bandwidth vs energy spread growth from MBI. Solid line is the prediction from Eq. (20). Bottom left: Bunching spectra for different induced energy spreads, each averaged over 100 runs. Bottom right: Bunching reduction according to $e^{-\frac{1}{2}(a_E B_2)^2 \sigma^2_{\Delta p_{MBI}}}$.

a dipole bend magnet of length L_m is given in the steady state limit as [24],

$$\Delta p_{CSR}(z) = -\frac{2L_m}{\sigma_\gamma I_A (3R^2)^{1/3}} \int_{-\infty}^{z} \frac{dz'}{(z-z')^{1/3}} \frac{dI(z')}{dz'}, \tag{21}$$

where R is the bend radius. This expression is applicable in the regime $R/\gamma^3 \ll \sigma_z \ll R\theta^3/24$, where $\theta \ll 1$ is the bend angle. It is assumed that the current profile remains essentially unchanged throughout the bend. The energy change for a Gaussian current is [25, 26]

$$\Delta p_{CSR}(z) = -\frac{L_m I_0 \Gamma(\frac{2}{3})}{I_A \sigma_\gamma} \left(\frac{8}{3\sqrt{2}\sigma_z R^2}\right)^{1/3} \times e^{-z^2/2\sigma_z^2} H_{1/3}\left(-\frac{z}{\sqrt{2}\sigma_z}\right), \tag{22}$$

and $H_{1/3}$ is the Hermite polynomial. The instantaneous frequency then goes like $e^{-z^2/2\sigma_z^2} H_{4/3}(-z/\sqrt{2}\sigma_z)$, as shown in FIG. 1. The induced bandwidth constraint on the bunching from the CSR energy wake is then calculated to be

$$\sigma_{\varphi'_{CSR}}/\sigma_{k_E} \approx \eta \frac{L_m I_0}{I_A \sigma_\gamma (\sigma_z R^2)^{1/3}} \leq 1 \tag{23}$$

where again η depends on where the energy modulation occurs. This is a subtler point for CSR than for LSC because CSR occurs progressively throughout the chicane on the evolving phase space. In a symmetric four-dipole first chicane, CSR in the first pair of dipoles has

a smaller impact on the final bunching spectrum than CSR in the last two dipoles, simply because the phase space has not experienced the full shearing. Elegant simulations [27] with the steady-state model indicate that CSR in each of the last two dipoles has a comparable impact on the spectrum such that taking $\eta \approx 2a_E B_2$ in (23) approximately captures the overall impact on the bunching from the first chicane.

The CSR constraint can be related directly to the longitudinal dispersion, $R_{56}^{(1)} = 2\theta^2(L_D + 2L_m/3)$, where L_D is the drift length between the first and second dipoles. Eq. (23) then gives a rough limit on the peak value,

$$R_{56}^{(1)} \lesssim \left[\frac{\sigma_z}{6}\left(1+\frac{3L_D}{2L_m}\right)\left(\frac{I_A\gamma}{|n|I_0k_1}\right)^3\right]^{1/4}. \tag{24}$$

It is assumed that the chicanes are related by the harmonic number $R_{56}^{(2)} \approx |n|R_{56}^{(1)}/a_E$. From this perspective, chicanes with $L_D/L_m \gg 1$ are favorable because they allow larger values of dispersion without violating the constraint. For the LCLS-II beam at $a_E = 100$, Eq. (24) is only satisfied for the required $R_{56}^{(1)} \approx 7$ mm dispersion if $L_D/L_m > \mathcal{O}(10^2)$. This appears to be the most restrictive constraint if this type of dispersion element is used with a Gaussian beam.

In reality, the CSR effect may have transients and 3D effects that modify the description. For example, the current can be reduced if the bend angle is such that $\sigma_z \ll \theta\sigma_x$ within the dipole. On the other hand, large energy wakes generated in one dipole can be turned into density modulations in the following dipole, which drives a CSR instability inside the chicane. For simplicity in the analysis we therefore assume that the wakes are small enough that the instability does not develop, and that the CSR effect is purely an energy modulation. This is justified because the constraint on the bandwidth growth in (23) also indicates that the tolerable energy modulations are less than the slice energy spread.

VI. CONCLUSIONS

We have developed an description for the bunching in EEHG that enables the spatial-spectral bunching distribution and spectral moments to be simply calculated in the presence of energy structures on the beam. In particular, a general expression for the spectral bandwidth is derived for arbitrary energy structures and beam current profiles, and serves as a measure of tolerable energy modulations via their impact on the bunching spectral width. The description also applies to HGHG with one laser modulator and chicane turned off. In EEHG, we find that the bunching spectrum is particularly sensitive to energy distortions that develop on the electron beam during the harmonic up-conversion, such as within the first chicane or second modulator. Specific examples of LSC and CSR are studied with steady-state models, and we derive several constraints to maintain a near transform-limited bunching spectrum with beams that have a Gaussian current profile. In several instances the constraints appear highly restrictive, but we note that for the more typical flatter, non-gaussian current profiles of modern systems and with the effects of FEL lasing included, the constraints may be somewhat relaxed. This is especially true if the seed laser pulses are shorter than the electron beam, which naturally broadens the bunching bandwidth. A shorter seed pulse also samples smaller, more linear regions of the phase space. This is a topic of future study.

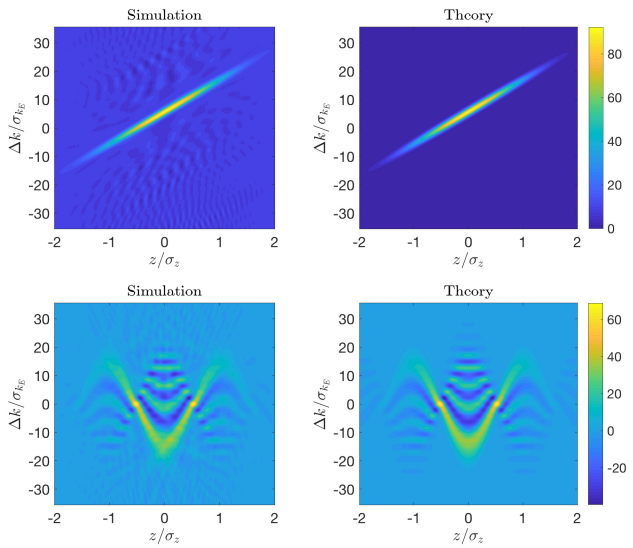

FIG. 4: Wigner distributions of bunching for a beam with linear and quadratic chirps [top row, Eq. (25)] with $\alpha = 4/\sigma_z$ and $\beta = 4/\sigma_z^2$, and a beam with a sinusoidal energy modulation [bottom row, Eq. (27)] with $k_0 = 3/\sigma_z$ and $\mu = -4$. The head is to the right.

VII. ACKNOWLEDGEMENTS

The author would like to thank W. M. Fawley for useful conversations and for pointing out the potential sensitivity issues to collective effects in the second echo stage, and S. Reiche, G. Stupakov, D. Ratner, and A. Marinelli for helpful discussions. This work was supported by the U.S. Department of Energy Contract No. DE-AC02-76SF00515 and the U.S. DOE Office of Basic Energy Sciences under award number 2017-SLAC-100382.

VIII. APPENDIX

Consider two examples of energy modulations with analytic solutions on a general beam with a Gaussian current profile, $f(z) = (2\pi\sigma_z^2)^{-1/2} e^{-z^2/2\sigma_z^2}$, for which the unperturbed bandwidth is $\sigma_{k_E} = 1/\sqrt{2}\sigma_z$. In the presence of a linear and quadratic energy chirp, the additional phase from (4) can be written as,

$$\varphi(z) = \alpha z + \beta z^2. \tag{25}$$

The instantaneous frequency is then $k_z(z) = k_E + \alpha + 2\beta z$ and induced bandwidth $\sigma_{\varphi'}^2 = 2(\beta\sigma_z)^2$. The Wigner distribution is then

$$W(z,k) = \frac{\bar{b}_{n,m}^2}{\sqrt{\pi}\sigma_z} e^{-z^2/\sigma_z^2 - \sigma_z^2(k-k_E-\alpha-2\beta z)^2} \tag{26}$$

Alternately, a sinusoidal energy modulation on the beam gives the phase

$$\varphi(z) = \mu \sin(k_0 z), \tag{27}$$

with $k_z(z) = k_E + \mu k_0 \cos(k_0 z)$ and $\sigma_{\varphi'}^2 = (\mu k_0)^2/2$ for $k_0 \gg 1/\sigma_z$. The Wigner distribution is

$$W(z,k) = \frac{\bar{b}_{n,m}^2}{\sqrt{\pi}\sigma_z} \sum_{n=-\infty}^{\infty} J_n(2\mu \cos k_0 z) \; e^{-z^2/\sigma_z^2 - \sigma_z^2(k-k_E-nk_0/2)^2}. \tag{28}$$

Figure 4 shows the Wigner distributions for both analytic examples as well as results from numerical particle simulations of EEHG bunching with the corresponding energy modulations imprinted on the beam in the second undulator, with $\sigma_z/c = 50$ fs and $b_{n,m} = 0.05$. The good agreement indicates that the approximations made in the analytic calculation of Δp_2 are reasonable in these instances. Parameters are chosen for illustration and clearly violate the bandwidth constraint in Eq. (9).

The first example in (25) is a linear frequency structure that is easily removable, at least in principle. The responsible quadratic beam chirp can be largely removed by phase space linearization, or used intentionally to produce compressible FEL pulses if the linear frequency chirp is maintained during amplification. The sinusoid exemplifies a type of nonlinear energy structure that could be used beneficially to produce coherent bunching sidebands [8, 10, 28], or conversely may compromise the FEL output if uncontrolled.

[1] G. Stupakov, Phys. Rev. Lett. **102**, 074801 (2009).

[2] G. Stupakov, Z. Huang, and D. Ratner, Proceedings of FEL 2010 Conference pp. 278–281 (2010).

[3] G. Stupakov, SLAC-PUB-14639 (2011).

[4] D. Ratner, A. Fry, G. Stupakov, and W. White, Phys. Rev. ST Accel. Beams **15**, 030702 (2012).

[5] G. Geloni, V. Kocharyan, and E. Saldin, *Analytical studies of constraints on the performance for eehg fel seed lasers* (2011), arXiv:1111.1615.

[6] Z. T. Zhao, D. Wang, J. H. Chen, Z. H. Chen, H. X. Deng, J. G. Ding, C. Feng, Q. Gu, M. M. Huang, T. H. Lan, et al., Nature Photonics **6**, 360 (2012).

[7] G. Penn, Phys. Rev. ST Accel. Beams **17**, 110707 (2014).

[8] P. Rebernik Ribič, E. Roussel, G. Penn, G. De Ninno, L. Giannessi, G. Penco, and E. Allaria, Photonics **4**, 19 (2017), ISSN 2304-6732.

[9] Z. Huang, D. Ratner, G. Stupakov, and D. Xiang, Proceedings of the 2009 Free-Electron Laser Conference p. 127 (2009).

[10] E. Hemsing, B. Garcia, Z. Huang, T. Raubenheimer, and D. Xiang, Phys. Rev. Accel. Beams **20**, 060702 (2017), URL `https://link.aps.org/doi/10.1103/PhysRevAccelBeams.20.060702`.

[11] Z. Huang, Proceedings of FEL 2006 Conference pp. 133–136 (2006).

[12] D. Xiang and G. Stupakov, Phys. Rev. ST Accel. Beams **12**, 030702 (2009).

[13] L. Cohen, *Time-frequency Analysis: Theory and Applications* (Prentice-Hall, Inc., Upper Saddle River, NJ, USA, 1995), ISBN 0-13-594532-1.

[14] J. M. Lilly and S. C. Olhede, IEEE Transactions on Signal Processing **58**, 591 (2010), ISSN 1053-587X.

[15] T. A. C. M. Claasen and W. F. G. Mecklenbräuker, Philips Journal of Research **35**, 217 (1980).

[16] Z. Huang, M. Borland, P. Emma, J. Wu, C. Limborg, G. Stupakov, and J. Welch, Phys. Rev. ST Accel. Beams **7**, 074401 (2004).

[17] G. Geloni, E. Saldin, E. Schneidmiller, and M. Yurkov, Nuclear Instruments and Methods in Physics Research Section A: Accelerators, Spectrometers, Detectors and Associated Equipment **583**, 228 (2007), ISSN 0168-9002, URL http://www.sciencedirect.com/science/article/pii/S0168900207020001.

[18] J. Rosenzweig, C. Pellegrini, L. Serafini, C. Ternieden, and G. Travish, Nuclear Instruments and Methods in Physics Research Section A: Accelerators, Spectrometers, Detectors and Associated Equipment **393**, 376 (1997), ISSN 0168-9002, free Electron Lasers 1996, URL http://www.sciencedirect.com/science/article/pii/S0168900297005160.

[19] K. Zhang, L. Zeng, Z. Qi, C. Feng, and D. Wang, Nuclear Instruments and Methods in Physics Research Section A: Accelerators, Spectrometers, Detectors and Associated Equipment **882**, 22 (2018), ISSN 0168-9002, URL http://www.sciencedirect.com/science/article/pii/S0168900217311439.

[20] E. Saldin, E. Schneidmiller, and M. Yurkov, Nuclear Instruments and Methods in Physics Research Section A: Accelerators, Spectrometers, Detectors and Associated Equipment **483**, 516 (2002), proceedings of the 23rd International Free Electron Laser Conference and 8th {FEL} Users Workshop.

[21] D. Ratner, C. Behrens, Y. Ding, Z. Huang, A. Marinelli, T. Maxwell, and F. Zhou, Phys. Rev. ST Accel. Beams **18**, 030704 (2015).

[22] G. Penn, Tech. Rep. NGLS Technical Note 35, LBNL (2012).

[23] H. Deng, W. Decking, and B. Faatz, *The echo-enabled harmonic generation options for flash ii* (2011), arXiv:1103.0112.

[24] E. Saldin, E. Schneidmiller, and M. Yurkov, Nuclear Instruments and Methods in Physics Research Section A: Accelerators, Spectrometers, Detectors and Associated Equipment **398**, 373 (1997), ISSN 0168-9002, URL http://www.sciencedirect.com/science/article/pii/S016890029700822X.

[25] P. Goldreich and D. A. Keeley, Astrophys. J. **170**, 463 (1971).

[26] I. S. Gradshteyn and I. M. Ryzhik, *Table of integrals, series and products* (Academic Press, 2000), sixth ed.

[27] M. Borland, Advanced Photon Source LS-287 (September 2000).

[28] E. Roussel, E. Ferrari, E. Allaria, G. Penco, S. Di Mitri, M. Veronese, M. Danailov, D. Gauthier, and L. Giannessi, Phys. Rev. Lett. **115**, 214801 (2015).